ACS SENSORS

pubs.acs.org/acssensors

Article

Antibody-Coated Wearable Organic Electrochemical Transistors for Cortisol Detection in Human Sweat

Silvia Demuru,* Jaemin Kim, Marwan El Chazli, Stephen Bruce, Michael Dupertuis, Pierre-Alain Binz, Mathieu Saubade, Céline Lafaye, and Danick Briand*

Cite This: *ACS Sens.* 2022, 7, 2721−2731

Read Online

ACCESS | Metrics & More | Article Recommendations | Supporting Information

ABSTRACT: The dysregulation of the hormone cortisol is related to several pathological states, and its monitoring could help prevent severe stress, fatigue, and mental diseases. While wearable antibody-based biosensors could allow real-time and simple monitoring of antigens, an accurate and low-cost antibody-based cortisol detection through electrochemical methods is considerably challenging due to its low concentration and the high ionic strength of real biofluids. Here, a label-free and fast sensor for cortisol detection is proposed based on antibody-coated organic electrochemical transistors. The developed devices show unprecedented high sensitivities of 50 μA/dec for cortisol sensing in high-ionic-strength solutions with effective cortisol detection demonstrated with real human sweat. The sensing mechanism is analyzed through impedance spectroscopy and confirmed with electrical models. Compared to existing methods requiring bulky and expensive laboratory equipment, these wearable devices enable point-of-care cortisol detection in 5 min with direct sweat collection for personalized well-being monitoring.

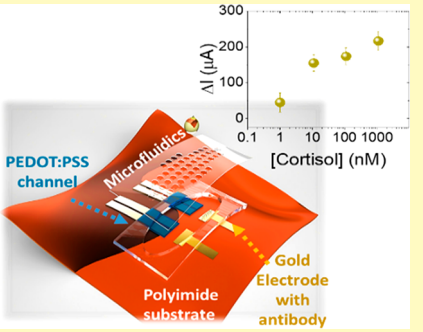

KEYWORDS: *organic electrochemical transistor, biosensor, cortisol detection, antibody, sweat analysis, wearable platform*

Wearables for the real-time monitoring of cortisol levels in human sweat have great potential for maintaining a healthy mental and physical condition.[1] Cortisol, a glucocorticoid hormone, is a biomarker regulated by the hypothalamic-pituitary-adrenal axis.[1,2] This hormone has a distinct circadian rhythm essential for human health, with the highest levels in the morning and the lowest at night.[3] Short-term modification of cortisol secretion can be adaptive responses of the body; however, chronic dysregulations are associated with a disrupted circadian rhythm and pathological conditions such as anxiety, depression, burnout, weaker immune system, chronic fatigue, and cardiovascular complications.[1−5]

A noninvasive and "stress-free" way being explored to determine cortisol is by analyzing the biofluid sweat.[1,6−8] Compared to standard methods of measurement, such as enzyme-linked immunosorbent assay (ELISA) or liquid chromatography-tandem mass spectrometry (LC-MS/MS),[9] a sensitive, selective, and simple to use wearable cortisol sensor for direct sweat collection on the skin could provide consistent measurements due to reduced sweat evaporation and the possibility of performing point-of-care monitoring,[4,10−12] for analyzing subjective physiological or stress-related variations.[13−15] Also, compared to the other noninvasively available fluids such as urine and saliva, sweat is the only one that can allow a continuous collection without human intervention with a wearable device.[9,16,17] Cortisol has a passive sweat transport, its concentration is sweat-rate independent,[18] and a good correlation between sweat and serum levels has previously been reported.[1] However, the correct quantification of normal and abnormal cortisol levels in sweat is challenging due to the high dilution of this steroid hormone, the high sweat ionic strength, and possible interferents (steroids, metabolites, drugs, or similar isomers).[19,20]

Recent technological advances with organic transistor-based biosensors are allowing the detection of molecules at low concentrations without the need for enzymatic labels and complex preparation procedures.[3,4,21] Transistors can play an essential role in wearable applications, thanks to their ability to amplify signals, and because they are simple to miniaturize and integrate into portable electronic devices. Organic electrochemical transistors (OECTs), having an electrolyte coupling the gate with a conducting polymer channel, were proposed as biosensors for low-cost and fast diagnosis.[22−26] Compared to other types of transistors, in OECTs the ions from the electrolyte permeate into the channel, typically made of poly(3,4-ethylenedioxythiophene) doped with poly(styrenesulfonate) (PEDOT:PSS), once a gate voltage is applied.[27] This phenomenon causes a volumetric change of the doping state, with significant modulations of drain current at

Received: June 13, 2022
Accepted: August 29, 2022
Published: September 2, 2022

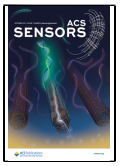

https://doi.org/10.1021/acssensors.2c01250
ACS Sens. 2022, 7, 2721−2731

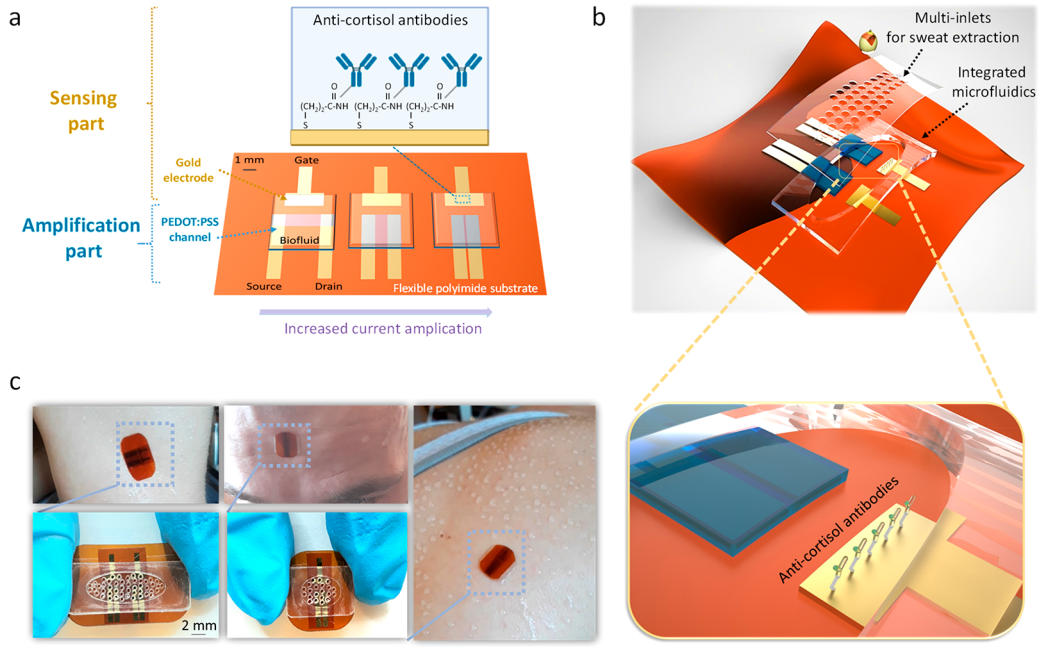

Figure 1. Organic transistor structure and sticker application. (a) Schematic of the biosensing principle involved and structure of the OECT devices, including antibody-coated gate electrodes and the organic PEDOT:PSS channel for current amplification; the latter shows three OECT devices with different PEDOT:PSS channels of an increased width per length ratio. (b) 3D-image with two OECTs integrated into a microfluidic system for direct sweat collection and zoom of the gate electrode with the anticortisol antibody immobilized. (c) Application of cortisol sensing sticker on the human skin for sweat collection during sports activities; the microfluidic part with the multiple inlets is placed in contact with the skin.

low gate voltages and very high signal amplification.[28,29] The devices can be used as biosensors by integrating a biorecognition layer either at the gate/electrolyte or at the electrolyte/channel interfaces.[30−32]

OECTs with antibodies or aptamers immobilized on the gate electrode are reported as promising biosensor configurations for sensing COVID-19 spike proteins or immunoglobulin G (using nanobody[22] or standard antibody[23]), rabbit immunoglobulin G (standard antibody[33]), interleukin-6 (standard antibody[34]), and epinephrine (aptamers[35]). The main advantage of using antibodies is that they can be produced easily for a wide range of sensing applications, while producing aptamers for several targets is still challenging.[36] One of the main difficulties of detecting cortisol using antibodies is that it does not carry any electrical charge,[3,4] making its detection particularly problematic. Cortisol detection with an OECT transducer was only achieved so far by using a molecularly imprinted membrane (MIP) as functionalization, not located on the gate but on the PEDOT:PSS channel, exhibiting a sensitivity of 2.68 μA/dec in the range of 10−10000 nmol/L (nM).[4] Their device was tested by collecting sweat on the skin of one subject during exercise, measuring two relatively high cortisol concentrations equal to ∼400 nM, with these values confirmed by a standard ELISA measurement performed on sweat samples collected simultaneously.

Here, we report on fully integrated OECTs on flexible substrates with monoclonal anticortisol antibody-coated gold gate electrodes to detect low concentrations of cortisol in 5 min. Our OECT sensors are optimized for enhanced current amplification, reaching a high sensitivity to cortisol of about 50 μA/dec in the 1−1000 nM concentration, with a limit of detection of 100 pM, making them relevant for real sweat analysis.[1,9] Through electrochemical impedance spectroscopy measurements on the biofunctionalized gate electrodes, we have identified as the main transducing mechanism that the cortisol binding events result in a variation of double-layer capacitances at the gate interface. By implementing the capacitance values into an electrical analytical model for the electrochemical transistors, we show that the predicted sensitivity matches the experimental data. Finally, the OECT sensors were used to determine cortisol in real sweat samples, with results compared to a method using LC-MS/MS. The wearable sensors can be implemented as stickers-on-the-skin for direct sweat collection and fast measurements of the stress-biomarker cortisol in sweat.

RESULTS AND DISCUSSION

Devices and Electrical Measurements. The architecture of the all-integrated, planar organic transistors on flexible foil and their biosensing principle is presented in Figure 1. The sensing part of the devices is composed of an evaporated gold gate, functionalized through a standard thiol process for the binding of antibodies,[37] and the amplification part comprises an inkjet-printed PEDOT:PSS organic channel.[38] The antibody employed is a commercial monoclonal anticortisol antibody, but the same process and device structure could be used for any other sensing applications involving antibodies. Two inert gold electrodes, used as source and drain, establish contact with the PEDOT:PSS material defining the channel length. Modifying the PEDOT:PSS geometry by varying the ratio of channel width (W) versus length (L) (Figure 1a) leads to a different current amplification for the same binding events at the gate electrode. Three different W/L channel ratios were evaluated, equal to 0.25 (W = 1 mm, L = 4 mm), 1.5 (W = 3 mm, L = 2 mm), and 12.5 (W = 3 mm, L = 0.24 mm), named

https://doi.org/10.1021/acssensors.2c01250
ACS Sens. 2022, 7, 2721−2731

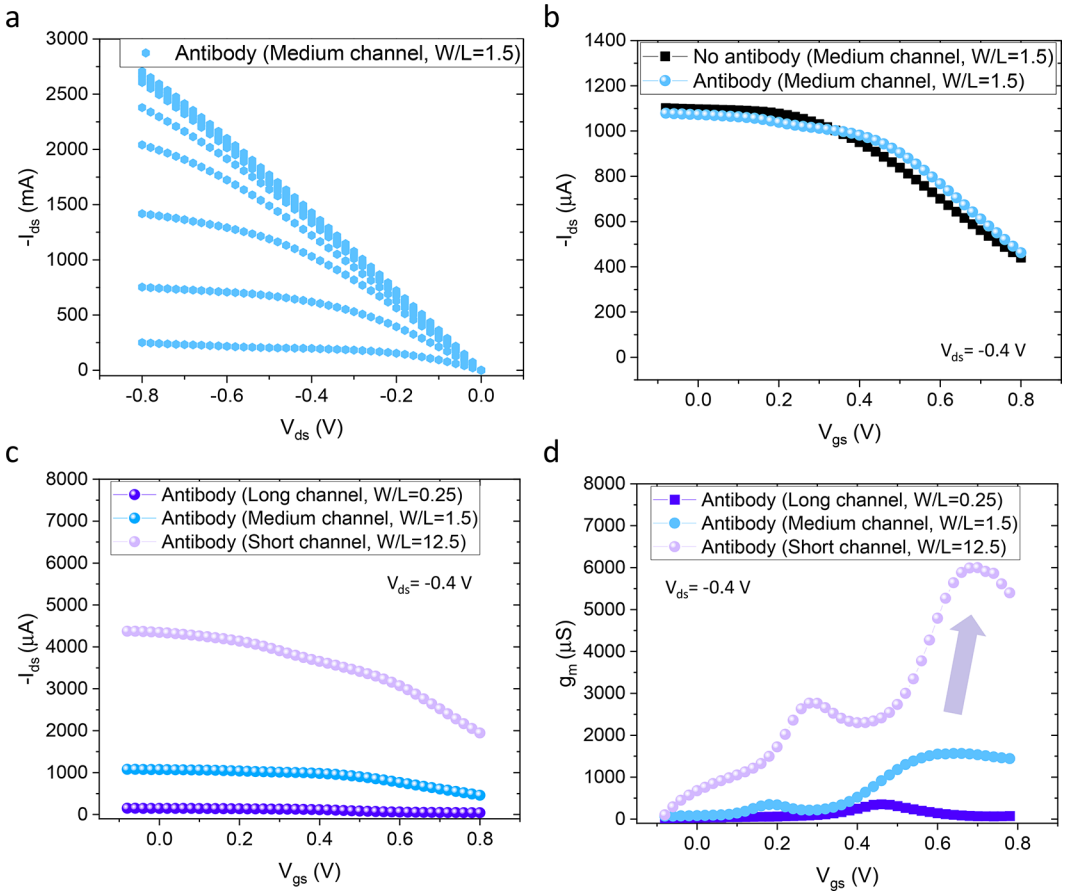

Figure 2. Organic transistor electrical characteristics. (a) Output characteristics with a V_{gs} voltage sweep from −1 to 1 V with a step of 0.25 V for devices having the anticortisol antibody on the gate electrode and a PEDOT:PSS W/L = 1.2. (b) Comparison of transfer characteristics without and with antibodies, for a fixed PEDOT:PSS W/L = 1.2 and a fixed drain voltage V_{ds} = −0.4 V. (c) Multiple transfer characteristics for devices with all the different W/L and antibody on the gate, and (d) respective transconductance g_m. The tests are in PBS 1× (0.15 M), pH 7.

long channel, medium channel, and short channel devices, respectively. The thickness (t) of the PEDOT:PSS layer was 101 ± 17 nm (n = 3).

Our devices on flexible foils can be easily processed, separating the gate to the channel during the gate functionalization steps and subsequently assembling them through double-sided adhesives (Figure S1a,b). The separation of the gate prevents damaging the organic PEDOT:PSS channel during the multiple incubation and washing steps required for the antibody immobilization. A flexible microfluidic system can be implemented, through the lamination of a combination of plastic and adhesive layers (Figure S1c,d), for performing sweat collection on people as shown in Figures 1b,c. A rigid reservoir can also be used to confine the electrolyte solution during laboratory experiments (Figure S1c,e). The OECT sensors with the microfluidics integrated can be applied as skin-sticker to collect the electrolyte thanks to the presence of multiple inlets on the surface, trapping the liquid through capillary action (Figure S1f,g).

To confirm the formation of the thiol monolayer and the binding of the antibodies, the gates are characterized with X-ray photoelectron spectroscopy (XPS) (Figure S2). The significant increase of the S 2p peak (Figure S2a) and the N 1s peak (Figure S2b) with thiols and antibodies on the surface shows the successful surface modification and immobilization of the capture antibody on the gold gates.[1] After the functionalization, the typical peak S 2p peak at 163.8 eV confirms the formation of the thiol monolayers,[39] and the typical N 1s peak with the antibody at 400.27 eV confirms the presence of the amide nitrogen atoms.[40] The S 2p element was quantified to increase from 4.3% (Au:S atom ratio 22.3) before the functionalization to 16.5% (Au:S atom ratio 5.07) after thiols and to 33.4% (Au:S atom ratio 1.99) after antibodies, and the N 1s element from 6.5% (Au:N atom ratio 14.5) before the functionalization and 3.63% (Au:N atom ratio 26.5) with thiols to 60.3% (Au:N atom ratio 0.658) after antibodies.

In the presence of the electrolyte solution and with the conducting channel biased (V_{ds}), the I_{ds} current decreases once a positive voltage is applied at the gate (V_{gs}). This behavior can be well observed in the electrical characteristics of the fabricated devices reported in Figure 2 and Figure S1, including the output (Figure 2a, Figure S1g,h) and transfer (Figure 2b,c) characteristics and the amplification of the devices (Figure 2d). The latter intrinsic amplification is defined as the transconductance g_m, equal to $\frac{\Delta I_{ds}}{\Delta I_{gs}}$. The on−off ratio of the devices is relatively low, as commonly reported for OECTs with polarizable gold gates.[41] However, the g_m is the main figure-of-merit in OECTs applied for biosensing, having a gold gate that can be easily functionalized. The voltage ($V_{gs,max}$) at which the maximum peak ($g_{m,max}$) appears can be selected for obtaining the maximum sensitivity for the detection of the analyte of interest.[4,24,42]

https://doi.org/10.1021/acssensors.2c01250
ACS Sens. 2022, 7, 2721−2731

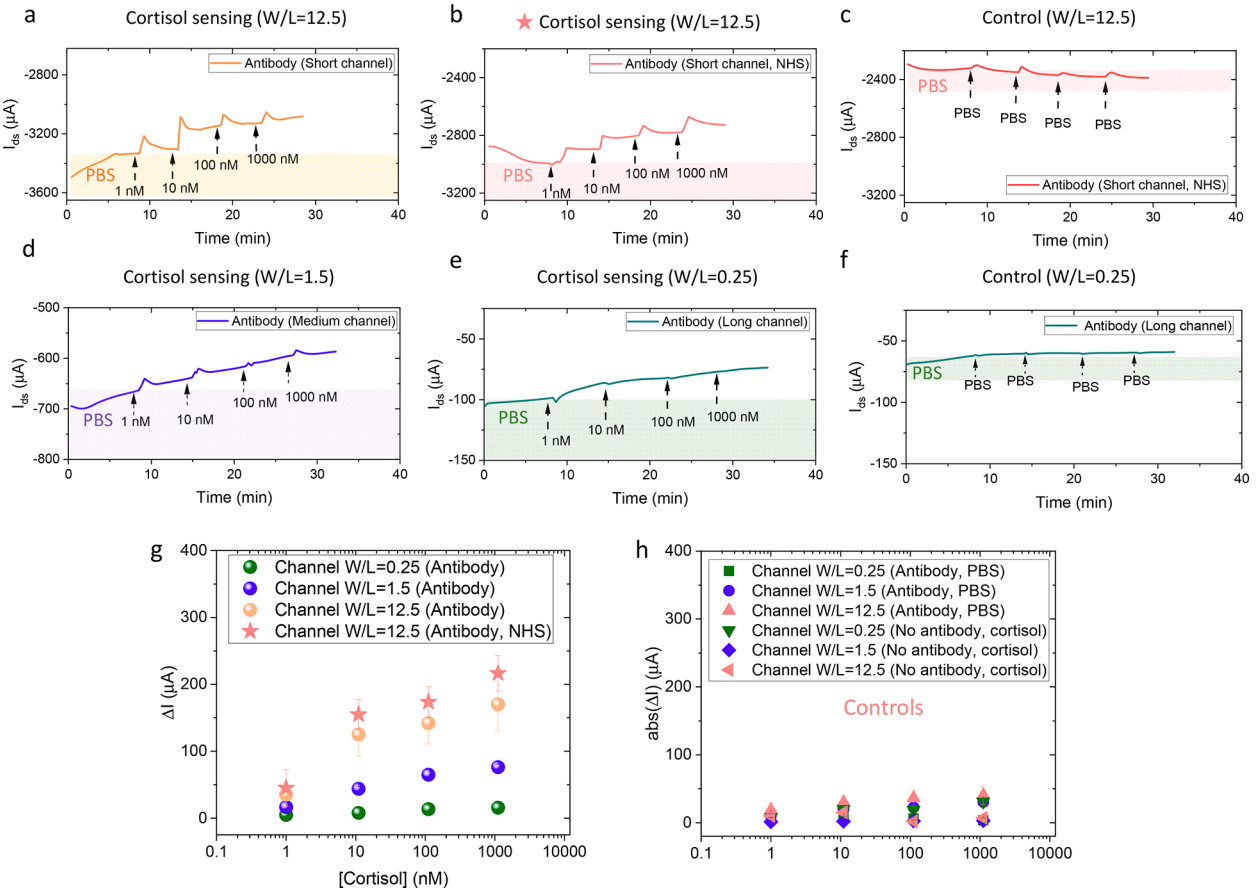

Figure 3. Real-time cortisol sensing responses. (a) Cortisol measurement with PEDOT:PSS W/L = 12.5 and thiol/EDC/antibody gate chemistry. (b) Cortisol measurement with PEDOT:PSS W/L = 12.5 and thiol/EDC/NHS/antibody gate chemistry. (c) Control measurement with multiple PBS injections with PEDOT:PSS W/L = 12.5 and thiol/EDC/antibody gate chemistry. (d) Cortisol measurement with PEDOT:PSS W/L = 1.5 and thiol/EDC/antibody gate chemistry. (e) Cortisol measurement with PEDOT:PSS W/L = 0.25 and thiol/EDC/antibody gate chemistry. (f) Control measurement with multiple PBS injections with PEDOT:PSS W/L = 0.25 and bare gold gates. (g) Calibration curves at the multiple sensing conditions (n = 4 for the short and medium channel, n = 3 for the long channel devices), and (h) multiple control measurements (n = 5 for the devices without antibody, n = 5 for short channel with antibody, and n = 2 for the medium and long channel devices with antibody). The tests are at a fixed drain voltage V_{ds} = −0.4 V and gate voltage V_{ds} = 0.6 V.

It can be observed from the transfer characteristics of the gold-gated OECTs that the $g_{m,max}$ and its relative $V_{gs,max}$ increase with the geometrical factor W/L, as previously reported for silver-gated devices.[38] Here we push these analyses by comparing gold gates with and without immobilized antibodies. Interestingly, the presence of antibodies on the gate electrode does not modify the current modulation effect of the transistors (Figure 2a,b). However, the presence of two g_m peaks (Figure 2d) can be seen, with a small peak between 0.2 and 0.3 V. This small peak is due to the formation of the thiol monolayers on the surface,[43] while before the thiol functionalization only the main g_m peak at $V_{gs,max}$ close to 0.6 V is present, as can be seen in Figure S3. The devices functionalized with antibodies had a thiol activation of the carboxylic groups with the chemical 1-ethyl-3-(3-diamino)propyl-carbodiimide (EDC), and the use of both EDC and *N*-hydroxysulfosuccinimide (NHS) chemistry did not modify the electrical properties of the devices (Figure S4).

From the long to medium channels, the geometrical factor W/L is increased by 6 times, and from medium to short by 8 times. The g_m increased by approximately 5 times (~400 mS to ~2 mS) and 4 times (~2 mS to ~6 mS), for these respective channel variations. While the initial variation of $g_{m,max}$ is almost linear with the W/L ratio as generally reported,[44] a saturation of g_m from medium to short channels occurs. Such a $g_{m,max}$ saturation phenomenon was already observed and confirmed with simulations for unfunctionalized devices.[38] It was shown to be related to the more significant parasitic contact resistance for small channel designs.

Cortisol Biosensing. The OECTs with the multiple PEDOT:PSS channel designs (long, medium, and short channels) were tested in real-time at different cortisol concentrations (Figure 3) to study how the geometrical and g_m variations influenced the sensitivity of the devices. All the sensors had an EDC thiol activation before the antibody immobilization on the gate, while the devices with NHS on the label had both EDC/NHS chemistry. Some devices were tested without antibodies on the gate and PBS-only blank solutions as control measurements. The devices were operated at V_{gs} equal to 0.6 V, close to the $V_{gs,max}$, and V_{ds} −0.4 V. The cortisol concentrations tested were 1, 10, 100, and 1000 nM in PBS 1× (0.15 M, pH 7). The measurement starts in PBS-only as a baseline, and then cortisol in PBS was added each time for 5 min per injection. An initial drift of the baseline signal is often observed possibly due to ionic interactions at the gate or channel interfaces, which was stabilized in all the cases in less

https://doi.org/10.1021/acssensors.2c01250
ACS Sens. 2022, 7, 2721−2731

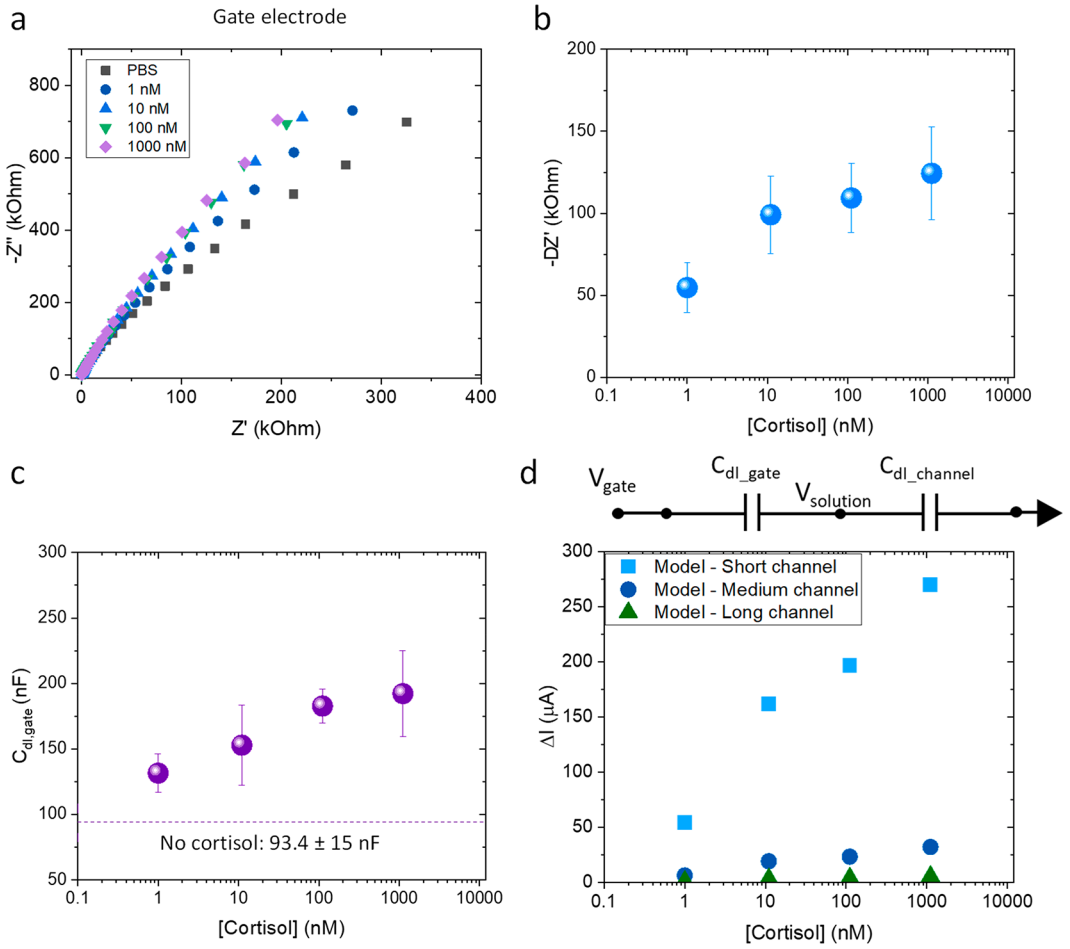

Figure 4. Sensing mechanism analysis. (a) Nyquist plots of the gate electrode tested at the different cortisol concentrations versus an Ag/AgCl wire (V_{dc} = 0.6 V, V_{ac} = 10 mV, frequency = 10^5–0.1 Hz). (b) Extracted variations of the real part of the impedance from the Nyquist plots at 0.1 Hz (n = 3). (c) Extracted variations of double-layer capacitances from the equivalent circuit. (d) Simulated current variations per decade of cortisol concentrations extracted from the simplified OECT capacitance model. The error bars represent the standard deviation from the average obtained from three devices. The impedance spectroscopy was performed in PBS 1× (0.15 M) following 5 min of incubation at the desired cortisol concentration. The gate electrodes had thiols/EDC/NHS/antibody on their surfaces.

than 10 min. The tests were performed with a reservoir fixed on the sensor, exposing the sensor to 50 μL of solution at the fixed concentration after removing the previous solution.

Roughly 1 min following an increase in cortisol concentration, a significant decrease of I_{ds} current was observed in real-time for the sensing devices with the anticortisol antibody on the gold gate (Figure 3a,b,d,e). The sensitivity for the real-time cortisol measurements was extracted as the variation of drain current from the baseline, $\Delta I = I_{ds,cortisol} - I_{ds,0}$, per order of magnitude of cortisol concentration, as reported in Figure 3g. The error bars in the graphs (Figure 3g,h) represent the standard deviation from the average obtained from multiple devices, with the exact number (n) written for each case in the following lines.

The increase of sensitivity with the increase of the ratio W/L matched well the variation of transconductance, with an increase of sensitivity of ∼3 and 5 times, from long to medium and from medium to short channels, respectively. Sensitivities of 3.7 ± 0.4 μA/dec (R^2 = 0.99, n = 4) and 17.7 ± 2 μA/dec (R^2 = 0.99, n = 3) were obtained from fitting the medium channel and the long channel responses in Figure 3g, respectively. The extracted sensitivities for the short channel devices (n = 4) were similar for both tested chemical processes, reaching high values of 51.0 ± 14 μA/dec (R^2 = 0.9) when functionalized with EDC/NHS and 51.2 ± 8 μA/dec (R^2 = 0.95) with EDC-only.

Multiple measurements performed on control devices with and without antibodies show that the high current variations originate from the antibody–antigen binding events. The devices with antibodies showed a small change of current for multiple PBS injections without cortisol (Figure 3c,f,h and Figure S5a) and without antibodies for the different cortisol concentrations (Figure 3h and Figure S5b–d). These variations are reported in absolute values since the control devices showed an increase or a decrease of current with the injections depending on the device. Without antibodies, the variations were 1.9 ± 1 μA/dec (n = 5), while the changes observed on devices having the gate functionalized and tested following multiple blank injections were 6 ± 2 μA for the long channels (n = 2), 6 ± 7 μA/dec for the medium channel (n = 2), and 7 ± 1 μA/dec for the short channel (n = 5). In all cases, the variations in current observed on the control devices are considerably low.

All the devices exhibited a leakage current I_{gs} of ∼100 nA, 4 orders of magnitude lower than the I_{ds} current for short channels, remaining stable or observing a small increase with

https://doi.org/10.1021/acssensors.2c01250
ACS Sens. 2022, 7, 2721–2731

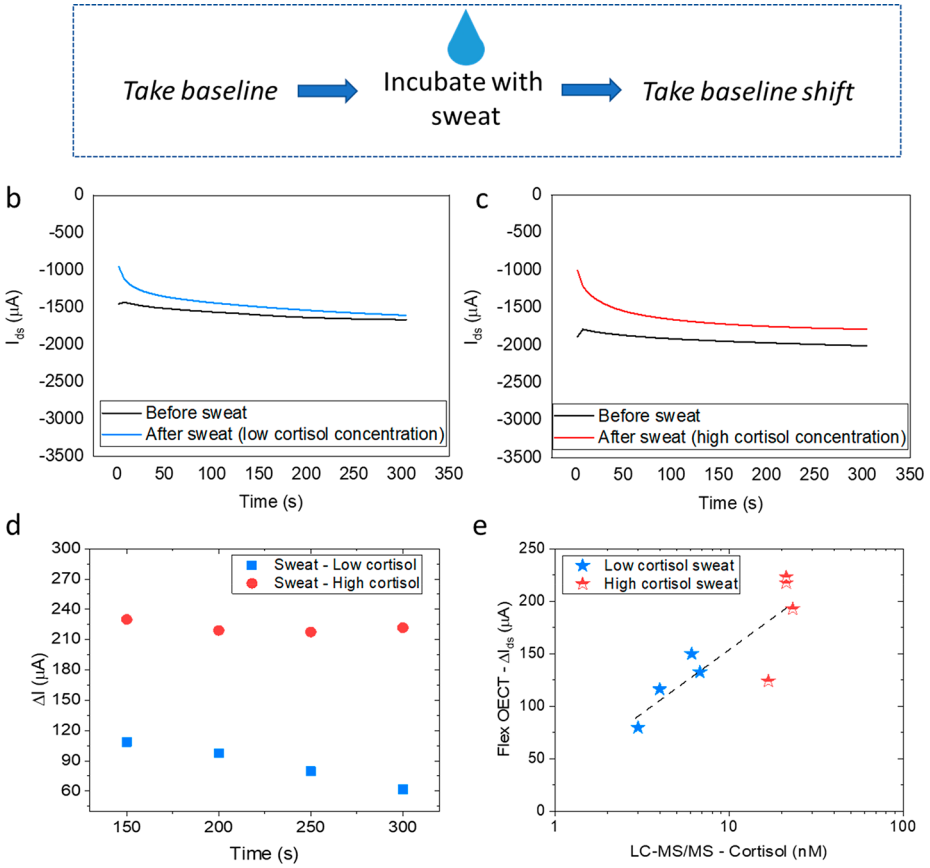

Figure 5. Real sweat testing. (a) Schematic of the protocol followed to test real sweat samples collected during indoor cycling and validated with liquid chromatography-tandem mass spectrometry. (b) Time response of the device at low cortisol concentration. (c) Time response of the device at high cortisol concentration. (d) Extracted variations drain current through the baseline shift before and after the sweat sample. (e) Comparison with the values measured by LC-MS/MS and the OECTs current variations measured after 250 s of stabilization. The OECT tests are at a fixed drain voltage V_{ds} = −0.4 V and gate voltage V_{ds} = 0.6 V.

the first cortisol injection while experiencing a slight decrease after the stabilization phase of 5 min, as reported in Figure S6.

Among all the tested conditions, the channels with the smallest ratio and an EDC/NHS chemistry showed the highest sensitivity; hence they were selected for further testing. It can also be seen that the sensitivity tends to saturate at higher concentrations. However, previous works report physiological cortisol concentrations in the ∼1−20 nM ranges,[1,9] in the lower concentration ranges tested before saturation, making the devices suitable for being applied for real sweat analysis.

Sensing Mechanism. To investigate the detection mechanism of the OECT devices, we analyzed the antibody-coated gate electrodes by electrochemical impedance spectroscopy (EIS) (Figure 4a). The Nyquist plots show a significant impedance change at the gate interface at the different cortisol concentrations after 5 min incubations. We can observe a considerable impedance variation at 0.1 Hz (lowest frequency, Figure 4b) of ∼60 kOhm/dec (R^2 = 0.93, n = 3). The error bars represent the standard deviation from the average obtained from the three tested devices. These variations in the Nyquist plot are similar as previously reported for the antibody−antigen detection of cortisol for a different electrode material (molybdenum disulfide).[45] On the other hand, control devices incubated with PBS-only for 5 min exhibited a minimal impedance change at the same conditions (Figure S7a).

A typical Bode plot for the sensing devices is shown in Figure S7b, where there is a clear variation of phases at low frequency. Using the equivalent circuit in Figure S8a, with a constant phase element (CPE) for taking double-layer nonidealities and a Warburg element representing the ionic diffusion,[46,47] the CPE values before and after the multiple cortisol concentrations were extracted (Figure S8b). According to the mathematical definition, it is possible to determine the actual capacitance from the R_{ct}−CPE parallel circuit using the following equation:[48]

$$R_{ct}\mathrm{CPE} = \tau^n = (R_{ct}C_{dl})^n \quad (1)$$

Rearranging this formula, the double-layer capacitance (C_{dl}) values were calculated as follows:

$$C_{dl} = \frac{(R_{ct}\mathrm{CPE})^{1/n}}{R_{ct}} \quad (2)$$

In eqs 1 and 2, n is the phase angle of the CPE element, τ is the time constant, and R_{ct} the charge-transfer resistance in parallel. The extracted C_{dl} values for each cortisol injection are reported in Figure 4c, showing an increase of capacitance with the injections equal to 25 ± 2 nF/dec (n = 3). Considering that the gate area is 0.3 × 0.1 cm^2, the variation of capacitance is 0.8 ± 0.07 μF/cm^2·dec, similar as previously reported using other types of electrodes coated with antibodies for cortisol detection.[49]

https://doi.org/10.1021/acssensors.2c01250
ACS Sens. 2022, 7, 2721−2731

To analyze how the variation of double-layer capacitance is amplified in the OECT configuration, a simplified OECT capacitive model can be employed to calculate the theoretical voltage in the solution considering the measured changes in gate capacitance and the capacitance of the channel.[50,51] This model, introduced by Bernards and Malliaras,[52] allows to use of standard thin-film transistor theory to calculate the theoretical I_{ds} current variations depending on the measured gate capacitance variations, applying the following formula in the linear regime:[53]

$$I_{ds} = \frac{Wt}{L}\mu C_v\left[(V_T - V_{gs})V_{ds} + \frac{{V_{ds}}^2}{2}\right] \quad (3)$$

where $\frac{Wt}{L}$ is the geometrical factor, μ the hole mobility, C_v the volumetric capacitance, and V_T the threshold voltage, defined as $V_T = V_{pinch-off} - V_{solution}$. The pinch-off voltage $V_{pinch-off}$ in eq 3 is equal to $\frac{qp_0}{C_v}$, with q being the elementary charge (1.6×10^{-19} C) and p_0 the intrinsic doping of the organic material (1.8×10^{20} cm^{-3}).[33] The capacitive model is reported in Figure 4d, and the solution voltage to be included in eq 3 can be calculated using the formula for a voltage divider:

$$V_{solution} = \frac{Z_{channel}}{Z_{gate} + Z_{channel}} V_{gs} = \frac{V_{gs}}{1 + \frac{C_{dl,channel}}{C_{dl,gate}}} \quad (4)$$

where $Z_{channel/gate}$ is the respective impedance at the interface, simplified as a purely capacitive element. The volumetric capacitance C_v of the PEDOT:PSS material was also extracted from the impedance spectroscopy measurements (Figure S9), and it is equal to about 24 F/cm^3, in agreement with previously reported values.[33] Considering that the term $\frac{Wt}{L}\mu C_v$ in eq 3 is equivalent to $\frac{G}{V_p} = \frac{g_m}{V_d}$, and $G = \frac{Wt}{L}\mu q p_0$ being the conductance of the organic material,[54] the hole mobility was estimated to be 6 cm^2 V s^{-1}, similar to previously reported PEDOT:PSS values.[33] For the different channel geometries, the $C_{dl,channel}$ values are then 2 μF for the short channel (volume 0.072 cm^3), 14 μF for the medium channel (volume 0.6 cm^3), and 10 μF for the long channel (volume 0.4 cm^3). Substituting the extracted $C_{dl,channel}$ values and the $C_{dl,gate}$ gate values for multiple cortisol concentrations in eq 4, and the previously mentioned parameters into the drain current eq 3, the ΔI_{ds} variations per decade of cortisol changes in Figure 4d are obtained.

The extracted ΔI_{ds} from the model are equal to 67 ± 9 μA/dec for the short-channel, 8 ± 1 μA/dec for the medium-channel, and 1 ± 0.2 μA/dec for the long-channel OECTs. The R^2 coefficient from the linear fitting is equal to 0.97 in all cases. The values are similar to experimental ones, particularly for the short channel designs (~50 μA/dec), as shown by superimposing the results in Figure S10a. The smaller values obtained for medium channels (Figure S10b) could be due to the simplified capacitive model at the gate interface. On the other hand, the results confirm that an increase in double-layer capacitance causes the variation in drain current ΔI_{ds}, measured for our OECT configuration while experiencing cortisol binding events. These events transduce into a higher coupling with the PEDOT:PSS channel, decreasing the drain current due to the higher dedoping. While cortisol does not carry a charge, the anticortisol antibodies carry a negative charge at physiological pH.[55] Hence, the higher capacitance after the binding is possibly due to conformational changes,[19] increasing the charges on the surface of the gate electrode. This phenomenon needs to be further investigated toward a more standardized electrical modeling of antibody−antigen binding events in OECT devices.

Sweat Analysis. OECTs with short channels and EDC/NHS chemistry on the gate are validated with real sweat samples extracted during an indoor-cycling session (Figure 5). The testing protocol consists of first measuring the baseline current of the OECT devices in PBS 1×, incubating the integrated devices for 5 min with sweat samples, and finally measuring the baseline shift in PBS 1× (Figure 5a). The sweat cortisol concentrations were previously measured by liquid chromatography-tandem mass spectrometry (LC-MS/MS) to validate our I_{ds} measurements. The samples are defined as high-concentrated if the cortisol concentration is above 10 nM or low-concentrated below 10 nM. The time responses for two devices tested with low-concentrated (Figure 5b) and high-concentrated sweat cortisol (Figure 5c) are reported. The corresponding extracted ΔI_{ds} are reported in Figure 5d at different stabilization times. The responses, ΔI_{ds}, of the OECT sensors (at 250 s of stabilization) for several sweat samples are compared in Figure 5e with the results obtained using liquid chromatography-tandem mass spectrometry. The values reported are measured with a freshly made OECT device, each tested with a different sweat sample (n = 8).

The antibody-coated OECT devices correlate well with the sweat samples measured by LC-MS/MS. The t test (1-tailed), considering all the measured current variations and the respective measured values by LC-MS/MS, shows a p-value <0.001; hence, the correlation between the variation in the OECTs and the LC-MS/MS measurements has high statistical significance. Then, the extracted Pearson coefficient of correlation r equals 0.84. It increases to 0.93, excluding the one less correlated point below the line (Figure 5e).

Considering our calibration measurements performed at different cortisol concentrations in PBS, a plot including the extracted I_{ds} variations with the sweat samples measured by LC-MS/MS and our calibration curve (n = 4) is presented in Figure S11. The limit of detection of our OECT sensors was measured to be 100 pM in PBS. The sensitivity slope measured detecting cortisol in real sweat (Figure 5e) is about two times higher than in PBS (Figure S11) for the OECT devices. This increase is measured because there are potential interfering species in sweat (steroids, metabolites, drugs, or similar isomers), making it difficult to accurately calibrate the OECT sensors in standard PBS. The values reported using portable electrochemical or colorimetric techniques are generally higher than values obtained with LC-MS/MS technique,[9,56] similarly to ELISA methods,[4,6,10] possibly due to the mentioned interfering species. Hence, our approach of measuring the ΔI_{ds} current variations in relation to LC-MS/MS measurements (Figure 5e) can be used to calibrate precisely anti-cortisol antibody-coated devices for real sweat applications.

The concentrations and variations in sweat depending on physiological/pathological conditions are still under investigation. Cortisol variations in sweat were studied during the day based on the circadian rhythms and before and after acute external stimuli triggering a stress response.[1] The variations during the day were investigated on four healthy subjects, measuring concentrations varying from ~13 nM in the

https://doi.org/10.1021/acssensors.2c01250
ACS Sens. 2022, 7, 2721−2731

morning to ∼7 nM in the afternoon. The stress response was tested on three subjects after a cold stressor test, finding an increase from ∼10 nM to ∼20 nM in one subject and lower variations in the other subjects. Similar values in the range of 2−20 nM are found also in our samples extracted during sports conditions. It is also reported to have normal sweat concentration levels in the range of about 0.7−8 nM at rest conditions.[9] In serum, concentrations higher than 690 nM are considered very high and associated with pathologies,[57] with some individuals arriving at ∼1200 nM. Hence, since sweat cortisol is reported to be ∼10−50 times lower than in serum,[1] during pathological conditions we could potentially reach concentrations in the 100 nM range in sweat. In any case, sweat variations should be monitored multiple times during the day to possibly identify pathological changes.

Thanks to the simplicity of the process, different OECT sensors could be used during the day to monitor cortisol variations. The measurements performed in real sweat effectively demonstrate the potential of our wearable OECT biosensor for direct sweat collection on the skin, enabling simple analysis of cortisol concentration with a single-shot measurement after a few minutes of incubation.

CONCLUSIONS

This work reports on integrated, antibody-coated organic electrochemical transistors for cortisol detection. Compared to the OECT state-of-the-art, our optimized sensor exhibits a higher sensitivity (20× at 50 μA/dec) and a wider dynamic range of 1−1000 nM, making it relevant for real sweat analysis. The sensitivity of the wearable OECT sensor was demonstrated after only 5 min of incubation using a fully integrated sensor, both with standard cortisol solutions and with real sweat. The correlation found between the OECT electrical models and the extracted impedance variations at the antibody-coated gate interface highlights the sensing mechanism involved, providing useful information for further optimization. The OECT sensor on flexible foil combined with the integrated microfluidic collection reservoir could effectively determine the concentration of the stress-biomarker cortisol with direct *in situ* sweat collection and measurement in a wearable fashion. Finally, this work also shows strategies to functionalize the devices without damaging the organic layer and integrate them into a fluidic system, which could also be applied to measure other antigens. Multiple organic transistors could be integrated into the same platform, including unfunctionalized and functionalized with different biolayers, toward multiplexed detection of analytes in various biofluids.

EXPERIMENTAL SECTION

Biofunctionalization. All the chemicals have been purchased from Sigma-Aldrich unless otherwise stated. The thiol monolayers on the gold electrodes were formed using 3-mercaptopropionic acid (3-MPA, ≥99%). A solution of 250 mM was always freshly prepared, adding 418 μL of 3-MPA in a total volume of DI water equal to 20 mL. About 50 μL of the diluted solution was left on the electrodes overnight. This step was followed by cleaning the electrodes with DI water and drying with a nitrogen gun. Then, the activation of the carboxylic groups for an amine reaction was performed, adding either 0.05 M of EDC (*N*-(3-(dimethylamino)propyl)-*N*-ethylcarbodiimide hydrochloride) or 0.05 M EDC + 0.03 M NHS (*N*-hydroxysuccinimide) in PBS, on the gold electrodes for 2 h. Precisely, 95.8 mg of EDC, with or w/o 34.5 mg of NHS, was added in a total volume of 10 mL of PBS. Subsequently, the electrodes were quickly rinsed with PBS and dried with a nitrogen gun, finally adding 5 μL of anticortisol antibody solution. The electrodes were left for 2 h at 4 °C in this condition. The anticortisol antibody was purchased from Abcam (Mouse monoclonal [XM210] to cortisol, AB1949) and diluted to a 300 μg/mL concentration in PBS.

The diluted antibody solution was separated into several aliquots and frozen before use. Then, after a washing step with the same PBS, the devices were tested for cortisol sensing. The PBS 1× solution was made using 0.001 M of monopotassium phosphate (KH_2PO_4), 0.15 M of NaCl, and 0.003 M of disodium phosphate (Na_2HPO_4). The X-ray photoelectron spectroscopy (XPS) measurements at the different functionalization steps were carried out on an Axis Supra (Kratos Analytical) using the monochromated Kα X-ray line from an aluminum anode. The samples were electrically insulated from the sample holder, and an electron flood gun was used to compensate for charging effects. The data were referenced at 84 eV with the Au 4f peak.

Device Fabrication. The OECTs are fabricated on a thin polyimide substrate (125 μm thick, DuPont Kapton HN) using a PEDOT:PSS ink for their organic channels (2 printed layers of ∼100 nm in thickness). Gold was evaporated for the gate and the source/drain contacts through a shadow mask (∼20 nm thick titanium or chromium adhesion layer/∼100 nm gold layer). The titanium layer showed higher stability in the transfer and impedance measurements compared to a chromium layer; hence, it was chosen for the final tests. After the gold evaporation, the PEDOT:PSS ink is deposited using a Dimatix DMP-2800 printer (Fujifilm) with 10 pL cartridges (DMC-11610). The ink is prepared by mixing a PEDOT:PSS solution (1.3 wt % in H_2O) with 5 vol % of dimethyl sulfoxide (DMSO). The mixture is sonicated for 10 min and then filtered with a 1 μm pore-size filter when filling the Dimatix cartridges. The substrate is treated with oxygen plasma before printing. The Dimatix plate is kept at 40 °C during the printing, and an annealing step is performed after at 120 °C for 20 min. The design includes a gate active area of about 3 × 1 mm^2 and three different channel areas of 1 × 4 mm^2, 3 × 2 mm^2, and 3 × 0.24 mm^2. The gap between the gate and the channel is about 1 mm, and the gold source and drain contacts have a respective length of 1 mm. The thicknesses of printed layers are measured with a Keyence VK-X1000 Series laser scanning microscope, with 150× magnification and laser mode. The gold gates on polyimide were made separately for their functionalization, and subsequently assembled in the OECT configuration using a double-sided acrylic adhesive (ARcare 92712) on polyimide. The OECTs are integrated into a flexible microfluidic system composed of PET foils (125 μm thick) and acrylic adhesives for the demonstrator on the skin. The PET foils were patterned using a CO_2 laser cutter (Trotec Speedy300) to define the shape of the microfluidic channel and the cover with the inlets (500 μm diameter). The PET fluidics system was made by lamination of the patterned PET channel with the PET top cover, bonded using the double-sided acrylic adhesive. The adhesive was used also to fix the fluidics system to the organic transistor arrays on polyimide substrate. On top of the multi-inlets cover, a double-sided medical-grade adhesive (ARcare 90445) shaped as the fluidic channel was added to contact the skin.

Electrochemical Testing. Cortisol (hydrocortisone, AB141250, Abcam) was used for the sensing measurements. An initial stock solution of 0.01 M was prepared in ethanol; then multiple concentrations (1 nM − 1 μM) of cortisol were prepared in PBS 1×, divided into aliquots, and frozen before use at −20 °C. The devices are tested using PMMA reservoirs containing the different electrolytes. The PMMA plates (3 mm thick) were cut with the CO_2 laser into a rectangular shape with 5 × 3 mm^2 gap and fixed onto the polyimide substrate through the double-sided acrylic tape. A total volume of 50 μL of solution in the reservoir was employed in all the tests. The protocol for the testing in real-time included an initial stabilization of the devices for ∼500 s in PBS 1×-only (no cortisol), then the removal of the solution with a pipet, and the addition of the PBS solutions containing cortisol for ∼300 s/concentration. Multiple cortisol solutions were tested in real-time with the same device, removing the previous solution and adding the new solution of an increased cortisol concentration. For the testing of the real sweat

https://doi.org/10.1021/acssensors.2c01250
ACS Sens. 2022, 7, 2721−2731

samples, the devices were first stabilized for ∼300 s in PBS-only, then incubated with the desired sweat sample (1 device/sweat sample) for ∼300 s, and washed with DI water, and then ∼300 s in PBS-only was added again for measuring current shift. The OECTs electrical measurements (electrical characteristics and time measurements) were acquired using a semiconductor parameter analyzer (Agilent 4155A). For the electrochemical impedance spectroscopy (EIS) measurements, a potentiostat/galvanostat (Multi Autolab M204, Metrohm) is employed. A gold electrode or a PEDOT:PSS electrode (with a gold contact) was used as the working electrode and a silver/silver chloride (Ag/AgCl) wire as the reference electrode. The frequency was swept from 10^5 to 0.1 Hz at an amplitude of 10 mV (V_{AC}). A polarization voltage (V_{DC}) of 0.6 V was used for the gold gate as the applied gate voltage during the sensing measurements. A V_{DC} of 0.1 V was used for the PEDOT:PSS electrode.

Sweat Collection. All eccrine sweat samples were handled in accordance with the approved ethical agreement *N*° 2019 01235 of the Canton of Vaud, Switzerland. All subjects gave written, informed consent before participation in the study. Sweat collection was done in an environment at 25.7 ± 1.1 °C and 49 ± 5% humidity. All sweat samples were collected using the absorbent patch method on the middle back of the subject. The sweat collection started after 10 min of biking to initiate sweating. The body regions were cleaned with alcohol, then deionized water, and dried with gauze pads before applying the absorbent patches onto these body regions. Each patch consisted of a sterilized nonwoven compress with a covered area of 112.5 cm^2 and an absorbing capacity of around 8.0 g (Promedical AG, Glarus, Switzerland). The patches are covered with an impermeable fabric and were fixed onto the skin in an airtight manner using a porous adhesive on top (nonwoven micropore tape 3 M Micropore, 3 M Company, St. Paul, USA). After 20 min of continuous cycling, to extract the sweat samples, patches were placed in the barrel of a plastic syringe and squeezed with a syringe plunger. Sweat was then conserved into a sealed tube at −20 °C before chemical analysis.

Liquid Chromatography-Tandem Mass Spectrometry. Calibrators, samples, and controls (1000 μL) were placed in Eppendorf tubes (2.0 mL); under a fume hood, the IS solution was then added to each tube (1000 μL), each one undergoing a short vortex. The tubes were centrifuged (20160 g, 5 min, 4 °C) then shortly stored at −80 °C (10 min). The resulting upper organic phase (800 μL) was transferred to a 96-well microplate; the samples were completely dried down under N_2 and then reconstituted by adding a solution of methanol:ultrapure H_2O 4:6 (75 μL), briefly agitated, and then centrifuged (3220 g, 5 min, RT). Samples were transferred to another 96-well microplate (700 μL well volume), sealed with a sealing mat, centrifuged (3220 g, 5 min, RT), and placed in the autosampler for liquid chromatography-tandem mass spectrometry (LC-MS/MS) analysis. The LC-MS/MS system is comprised of an ExionLC system coupled to a 6500+ Q-Trap mass spectrometer (SCIEX) with electrospray ionization operating in positive ion mode and operating in the multiple reaction monitoring (MRM) mode. The system was piloted by Analyst software (version 1.7.2). Samples were injected onto a Zorbax Eclipse Plus C18 column (2.1 × 50 mm, 1.8 μm, Agilent). The flow rate was 400 μL/min, and the column was placed in a column oven (30 °C). The mobile phase comprised ultrapure H_2O (A) and methanol with 0.001% formic acid (B). The starting mobile phase conditions were A = 60% and B = 40%, gradients were immediately employed: A = 50% and B = 50% (1.00 min), then A = 42% and B = 58% (5.50 min), A = 20% and B = 80% (7.00 min), A = 0% and B = 100% (8 min), which was held for a further 2 min, and then back to A = 60% and B = 40% (12.00 min) held for a final 2 min. The mass spectrometer ion spray voltage was set to 5500 V, with a curtain gas of 20.0 and a temperature of 600 °C. The transitions used in the scheduled MRM mode were as follows: 363.2/121.1 and 363.2/91.1 (quantifier and qualifier for cortisol, respectively) and 367.3/121.1 (d_4-cortisol). The declustering potential was 76 V, and the collision energy was 29 V for the quantifier transitions and 83 V for the qualifier. LC-MS/MS data processing was performed using SCIEX OS software (version 1.7.0.36606).

■ ASSOCIATED CONTENT

Supporting Information

The Supporting Information is available free of charge at https://pubs.acs.org/doi/10.1021/acssensors.2c01250.

OECT sensors fabrication and assembly, X-ray photoelectron spectra on gold gates, Thiol functionalization and characteristics, Different thiol activation, Control experiments, Leakage current, Impedance spectroscopy, Electrical circuit on the gate electrode, PEDOT:PSS impedance, OECT electrical model for cortisol sensing and experimental results, Calibration curve and sweat samples (PDF)

■ AUTHOR INFORMATION

Corresponding Authors

Silvia Demuru − *School of Engineering, Ecole Polytechnique Fédérale de Lausanne, Neuchâtel 2000, Switzerland;* orcid.org/0000-0003-2676-9785; Email: silvia.demuru@epfl.ch

Danick Briand − *School of Engineering, Ecole Polytechnique Fédérale de Lausanne, Neuchâtel 2000, Switzerland;* Email: danick.briand@epfl.ch

Authors

Jaemin Kim − *School of Engineering, Ecole Polytechnique Fédérale de Lausanne, Neuchâtel 2000, Switzerland*

Marwan El Chazli − *School of Engineering, Ecole Polytechnique Fédérale de Lausanne, Neuchâtel 2000, Switzerland*

Stephen Bruce − *Clinical Chemistry Laboratory, Centre Hospitalier Universitaire Vaudois, Lausanne 1011, Switzerland*

Michael Dupertuis − *Clinical Chemistry Laboratory, Centre Hospitalier Universitaire Vaudois, Lausanne 1011, Switzerland*

Pierre-Alain Binz − *Clinical Chemistry Laboratory, Centre Hospitalier Universitaire Vaudois, Lausanne 1011, Switzerland*

Mathieu Saubade − *Sports Medicine Unit, Centre Hospitalier Universitaire Vaudois, Lausanne 1011, Switzerland*

Céline Lafaye − *Sports Medicine Unit, Centre Hospitalier Universitaire Vaudois, Lausanne 1011, Switzerland*

Complete contact information is available at: https://pubs.acs.org/10.1021/acssensors.2c01250

Author Contributions

S.D. and D.B. conceived of and designed the experiments. S.D. designed, printed, and functionalized the devices and performed most of the electrochemical testing. M.E.C. contributed to the electrochemical tests. J.K. contributed to the fabrication of the OECT devices. C.L. performed the sweat samples extraction, and C.L and M.S. developed the relative protocol. B.S., M.D., and P.-A. B. developed the protocol and performed the measurements on the sweat samples with the liquid chromatography-tandem mass spectrometry instrument. S.D. and D.B. analyzed the experimental data and discussed the results. The manuscript was written by S.D. and reviewed by D.B.

Notes

The authors declare no competing financial interest.

https://doi.org/10.1021/acssensors.2c01250
ACS Sens. 2022, 7, 2721−2731

■ ACKNOWLEDGMENTS

The authors acknowledge the funding from SNF-SINERGIA under the project WeCare (No. CRSII5_177255) and SNF under the project 206021:164028: "Aerosol Jet Tool for Additive Manufacturing and 3D Printing for Microsystems". The authors wish to thank Dr. Peter van der Wal from EPFL for the useful advice on electrochemical analysis, and Dr. Mounir Mensi from EPFL for performing the XPS measurements.

■ REFERENCES

(1) Torrente-Rodríguez, R. M.; Tu, J.; Yang, Y.; Min, J.; Wang, M.; Song, Y.; Yu, Y.; Xu, C.; Ye, C.; IsHak, W. W.; Gao, W. Investigation of Cortisol Dynamics in Human Sweat Using a Graphene-Based Wireless MHealth System. *Matter* **2020**, *2* (4), 921−937.

(2) Ku, M.; Kim, J.; Won, J. E.; Kang, W.; Park, Y. G.; Park, J.; Lee, J. H.; Cheon, J.; Lee, H. H.; Park, J. U. Smart, Soft Contact Lens for Wireless Immunosensing of Cortisol. *Sci. Adv.* **2020**, *6* (28), 1−10.

(3) Sheibani, S.; Capua, L.; Kamaei, S.; Shirin, S.; Akbari, A.; Zhang, J.; Guerin, H.; Ionescu, A. M. Extended Gate Field-Effect-Transistor for Sensing Cortisol Stress Hormone. *Commun. Mater.* **2021**, *2* (10), 1−10.

(4) Parlak, O.; Keene, S. T.; Marais, A.; Curto, V. F.; Salleo, A. Molecularly Selective Nanoporous Membrane-Based Wearable Organic Electrochemical Device for Noninvasive Cortisol Sensing. *Sci. Adv.* **2018**, *4*, 1−10.

(5) Lee, M. A.; Wang, S.; Jin, X.; Bakh, N. A.; Nguyen, F. T.; Dong, J.; Silmore, K. S.; Gong, X.; Pham, C.; Jones, K. K.; Muthupalani, S.; Bisker, G.; Son, M.; Strano, M. S. Implantable Nanosensors for Human Steroid Hormone Sensing In Vivo Using a Self-Templating Corona Phase Molecular Recognition. *Adv. Healthc Mater.* **2020**, *9*, 2000429.

(6) Tang, W.; Yin, L.; Sempionatto, J. R.; Moon, J.; Teymourian, H.; Wang, J. Touch-Based Stressless Cortisol Sensing. *Adv. Mater.* **2021**, 2008465.

(7) Dalirirad, S.; Steckl, A. J. Aptamer-Based Lateral Flow Assay for Point of Care Cortisol Detection in Sweat. *Sens Actuators B Chem.* **2019**, *283*, 79−86.

(8) Cheng, C.; Li, X.; Xu, G.; Lu, Y.; Low, S. S.; Liu, G.; Zhu, L.; Li, C.; Liu, Q. Battery-Free, Wireless, and Flexible Electrochemical Patch for in Situ Analysis of Sweat Cortisol via near Field Communication. *Biosens Bioelectron* **2021**, *172*, 112782.

(9) Jia, M.; Chew, W. M.; Feinstein, Y.; Skeath, P.; Sternberg, E. M. Quantification of Cortisol in Human Eccrine Sweat by Liquid Chromatography − Tandem Mass Spectrometry. *Analyst* **2016**, *141*, 2053−2060.

(10) Kim, S.; Lee, B.; Reeder, J. T.; Seo, S. H.; Lee, S.-U.; Hourlier-Fargette, A.; Shin, J.; Sekine, Y.; Jeong, H.; Oh, Y. S.; Aranyosi, A. J.; Lee, S. P.; Model, J. B.; Lee, G.; Seo, M.-H.; Kwak, S. S.; Jo, S.; Park, G.; Han, S.; Park, I.; Jung, H.-I.; Ghaffari, R.; Koo, J.; Braun, P. V.; Rogers, J. A. Soft, Skin-Interfaced Microfluidic Systems with Integrated Immunoassays, Fluorometric Sensors, and Impedance Measurement Capabilities. *Proc. Natl. Acad. Sci. U. S. A.* **2020**, *117* (45), 27906−27915.

(11) Zhong, B.; Jiang, K.; Wang, L.; Shen, G. Wearable Sweat Loss Measuring Devices: From the Role of Sweat Loss to Advanced Mechanisms and Designs. *Advanced Science* **2022**, *9*, 2103257.

(12) Zhang, K.; Wang, J.; Liu, T.; Luo, Y.; Loh, X. J.; Chen, X. Machine Learning-Reinforced Noninvasive Biosensors for Healthcare. *Adv. Healthc Mater.* **2021**, *10*, 2100734.

(13) Boucher, P.; Plusquellec, P. Acute Stress Assessment From Excess Cortisol Secretion: Fundamentals and Perspectives. *Front Endocrinol (Lausanne)* **2019**, *10*, 1−12.

(14) Qi, M.; Gao, H.; Guan, L.; Liu, G.; Yang, J. Subjective Stress, Salivary Cortisol, and Electrophysiological Responses to Psychological Stress. *Front Psychol* **2016**, *7*, 1−9.

(15) Hill, E. E.; Zack, E.; Battaglini, C.; Viru, M.; Viru, A.; Hackney, A. C. Exercise and Circulating Cortisol Levels: The Intensity Threshold Effect. *J. Endocrinol. Invest. 31* **2008**, *31*, 587−591.

(16) Parrilla, M.; Guinovart, T.; Ferré, J.; Blondeau, P.; Andrade, F. J. A Wearable Paper-Based Sweat Sensor for Human Perspiration Monitoring. *Adv. Healthc Mater.* **2019**, *8*, 1900342.

(17) Lee, H.; Hong, Y. J.; Baik, S.; Hyeon, T.; Kim, D. H. Enzyme-Based Glucose Sensor: From Invasive to Wearable Device. *Adv. Healthc Mater.* **2018**, *7*, 1701150.

(18) Sonner, Z.; Wilder, E.; Heikenfeld, J.; Kasting, G.; Beyette, F.; Swaile, D.; Sherman, F.; Joyce, J.; Hagen, J.; Kelley-Loughnane, N.; Naik, R. The Microfluidics of the Eccrine Sweat Gland, Including Biomarker Partitioning, Transport, and Biosensing Implications. *Biomicrofluidics* **2015**, *9* (3), 031301.

(19) Macchia, E.; Manoli, K.; Holzer, B.; Di Franco, C.; Ghittorelli, M.; Torricelli, F.; Alberga, D.; Mangiatordi, G. F.; Palazzo, G.; Scamarcio, G.; Torsi, L. Single-Molecule Detection with a Millimetre-Sized Transistor. *Nat. Commun.* **2018**, *9* (3223), 1−10.

(20) Kesler, V.; Murmann, B.; Soh, H. T. Going beyond the Debye Length: Overcoming Charge Screening Limitations in Next-Generation Bioelectronic Sensors. *ACS Nano* **2020**, *14* (12), 16194−16201.

(21) Wang, B.; Zhao, C.; Wang, Z.; Yang, K.; Cheng, X.; Liu, W.; Yu, W.; Lin, S.; Zhao, Y.; Cheung, K. M.; Lin, H.; Hojaiji, H.; Weiss, P. S.; Stojanović, M. N.; Tomiyama, A. J. Wearable Aptamer-Field-Effect Transistor Sensing System for Noninvasive Cortisol Monitoring. *Sci. Adv.* **2022**, *8*, 1−16.

(22) Guo, K.; Wustoni, S.; Koklu, A.; Díaz-Galicia, E.; Moser, M.; Hama, A.; Alqahtani, A. A.; Ahmad, A. N.; Alhamlan, F. S.; Shuaib, M.; Pain, A.; McCulloch, I.; Arold, S. T.; Grünberg, R.; Inal, S. Rapid Single-Molecule Detection of COVID-19 and MERS Antigens via Nanobody-Functionalized Organic Electrochemical Transistors. *Nat. Biomed Eng.* **2021**, *5*, 666−677.

(23) Liu, H.; Yang, A.; Song, J.; Wang, N.; Lam, P.; Li, Y.; Law, H. K. W.; Yan, F. Ultrafast, Sensitive, and Portable Detection of COVID-19 IgG Using Flexible Organic Electrochemical Transistors. *Sci. Adv.* **2021**, *7*, 1−9.

(24) Pappa, A. M.; Curto, V. F.; Braendlein, M.; Strakosas, X.; Donahue, M. J.; Fiocchi, M.; Malliaras, G. G.; Owens, R. M. Organic Transistor Arrays Integrated with Finger-Powered Microfluidics for Multianalyte Saliva Testing. *Adv. Healthc Mater.* **2016**, *5* (17), 2295−2302.

(25) Yang, S. Y.; Cicoira, F.; Byrne, R.; Benito-Lopez, F.; Diamond, D.; Owens, R. M.; Malliaras, G. G. Electrochemical Transistors with Ionic Liquids for Enzymatic Sensing. *Chem. Commun.* **2010**, *46* (42), 7972−7974.

(26) Yaghmazadeh, O.; Cicoira, F.; Bernards, D. A.; Yang, S. Y.; Bonnassieux, Y.; Malliaras, G. G. Optimization of Organic Electrochemical Transistors for Sensor Applications. *J. Polym. Sci. B Polym. Phys.* **2011**, *49* (1), 34−39.

(27) Dorfman, K. D.; Adrahtas, D. Z.; Thomas, M. S.; Frisbie, C. D. Microfluidic Opportunities in Printed Electrolyte-Gated Transistor Biosensors. *Biomicrofluidics* **2020**, *14*, 011301.

(28) Malliaras, G. G.; Berggren, M.; Owens, R. M.; Rivnay, J.; Inal, S.; Salleo, A. Organic Electrochemical Transistors. *Nat. Rev. Mater.* **2018**, *3* (2), 17086.

(29) Leleux, P.; Rivnay, J.; Lonjaret, T.; Badier, J. M.; Bénar, C.; Hervé, T.; Chauvel, P.; Malliaras, G. G. Organic Electrochemical Transistors for Clinical Applications. *Adv. Healthc Mater.* **2015**, *4*, 142−147.

(30) Picca, R. A.; Manoli, K.; Macchia, E.; Sarcina, L.; Di Franco, C.; Cioffi, N.; Blasi, D.; Österbacka, R.; Torricelli, F.; Scamarcio, G.; Torsi, L. Ultimately Sensitive Organic Bioelectronic Transistor Sensors by Materials and Device Structures' Design. *Adv. Funct Mater.* **2019**, *30*, 014513.

(31) Kergoat, L.; Piro, B.; Berggren, M.; Horowitz, G.; Pham, M. C. Advances in Organic Transistor-Based Biosensors: From Organic Electrochemical Transistors to Electrolyte-Gated Organic Field-Effect Transistors. *Anal. Bioanal. Chem.* **2012**, *402*, 1813−1826.

https://doi.org/10.1021/acssensors.2c01250
ACS Sens. 2022, 7, 2721−2731

(32) Keene, S. T.; Fogarty, D.; Cooke, R.; Casadevall, C. D.; Salleo, A.; Parlak, O. Wearable Organic Electrochemical Transistor Patch for Multiplexed Sensing of Calcium and Ammonium Ions from Human Perspiration. *Adv. Healthc Mater.* **2019**, *8* (24), 1901321.
(33) Macchia, E.; Romele, P.; Manoli, K.; Ghittorelli, M.; Magliulo, M.; Kovács-Vajna, Z. M.; Torricelli, F.; Torsi, L. Ultra-Sensitive Protein Detection with Organic Electrochemical Transistors Printed on Plastic Substrates. *Flexible and Printed Electronics* **2018**, *3*, 034002.
(34) Gentili, D.; D'Angelo, P.; Militano, F.; Mazzei, R.; Poerio, T.; Brucale, M.; Tarabella, G.; Bonetti, S.; Marasso, S. L.; Cocuzza, M.; Giorno, L.; Iannotta, S.; Cavallini, M. Integration of Organic Electrochemical Transistors and Immuno-Affinity Membranes for Label-Free Detection of Interleukin-6 in the Physiological Concentration Range through Antibody-Antigen Recognition. *J. Mater. Chem. B* **2018**, *6* (33), 5400−5406.
(35) Saraf, N.; Woods, E. R.; Peppler, M.; Seal, S. Highly Selective Aptamer Based Organic Electrochemical Biosensor with Pico-Level Detection. *Biosens Bioelectron* **2018**, *117*, 40−46.
(36) Aleman, J.; Kilic, T.; Mille, L. S. Microfluidic Integration of Regeneratable Electrochemical Affinity-Based Biosensors for Continual Monitoring of Organ-on-a-Chip Devices. *Nat. Protoc.* **2021**, *16*, 2564−2593.
(37) Limbut, W.; Kanatharana, P.; Mattiasson, B.; Asawatreratanakul, P.; Thavarungkul, P. A Comparative Study of Capacitive Immunosensors Based on Self-Assembled Monolayers Formed from Thiourea, Thioctic Acid, and 3-Mercaptopropionic Acid. *Biosens Bioelectron* **2006**, *22* (2), 233−240.
(38) Paudel, P. R.; Kaphle, V.; Dahal, D.; Radha Krishnan, R. K.; Lüssem, B. Tuning the Transconductance of Organic Electrochemical Transistors. *Adv. Funct Mater.* **2020**, *31*, 2004939.
(39) Wu, Z.; Jiang, M.; Liu, Z.; Jamshaid, A.; Ono, L. K.; Qi, Y. Highly Efficient Perovskite Solar Cells Enabled by Multiple Ligand Passivation. *Adv. Energy Mater.* **2020**, *10*, 1903696.
(40) Holzer, B.; Manoli, K.; Ditaranto, N.; Macchia, E.; Tiwari, A.; di Franco, C.; Scamarcio, G.; Palazzo, G.; Torsi, L. Characterization of Covalently Bound Anti-Human Immunoglobulins on Self-Assembled Monolayer Modified Gold Electrodes. *Adv. Biosyst* **2017**, *1*, 1700055.
(41) Koutsouras, D. A.; Torricelli, F.; Gkoupidenis, P.; Blom, P. W. M. Efficient Gating of Organic Electrochemical Transistors with In-Plane Gate Electrodes. *Adv. Mater. Technol.* **2021**, 2100732.
(42) Ji, X.; Lau, H. Y.; Ren, X.; Peng, B.; Zhai, P.; Feng, S. P.; Chan, P. K. L. Highly Sensitive Metabolite Biosensor Based on Organic Electrochemical Transistor Integrated with Microfluidic Channel and Poly(N-Vinyl-2-Pyrrolidone)-Capped Platinum Nanoparticles. *Adv. Mater. Technol.* **2016**, *1* (5), 1600042.
(43) Sensi, M.; Berto, M.; Candini, A.; Liscio, A.; Cossarizza, A.; Beni, V.; Biscarini, F.; Bortolotti, C. A. Modulating the Faradic Operation of All-Printed Organic Electrochemical Transistors by Facile in Situ Modification of the Gate Electrode. *ACS Omega* **2019**, *4* (April), 5374−5381.
(44) Rivnay, J.; Leleux, P.; Ferro, M.; Sessolo, M.; Williamson, A.; Koutsouras, D. A.; Khodagholy, D.; Ramuz, M.; Strakosas, X.; Owens, R. M.; Benar, C.; Badier, J. M.; Bernard, C.; Malliaras, G. G. High-Performance Transistors for Bioelectronics through Tuning of Channel Thickness. *Sci. Adv.* **2015**, *1* (4), 1−6.
(45) Kinnamon, D.; Ghanta, R.; Lin, K. C.; Muthukumar, S.; Prasad, S. Portable Biosensor for Monitoring Cortisol in Low-Volume Perspired Human Sweat. *Sci. Rep* **2017**, *7* (1), 1−13.
(46) Criscuolo, F.; Taurino, I.; Kilic, T.; Carrara, S.; De Micheli, G. An Electrochemical Sensor for Quantitative Analysis of Rhesus D Antibodies in Blood. *Proceedings - 2017 7th International Workshop on Advances in Sensors and Interfaces, IWASI 2017* **2017**, 236−240.
(47) Vacca, A.; Mascia, M.; Rizzardini, S.; Corgiolu, S.; Palmas, S.; Demelas, M.; Bonfiglio, A.; Ricci, P. C. Preparation and Characterisation of Transparent and Flexible PEDOT:PSS/PANI Electrodes by Ink-Jet Printing and Electropolymerisation. *RSC Adv.* **2015**, *5* (97), 79600−79606.
(48) Shoar Abouzari, M. R.; Berkemeier, F.; Schmitz, G.; Wilmer, D. On the Physical Interpretation of Constant Phase Elements. *Solid State Ion* **2009**, *180*, 922−927.
(49) Munje, R. D.; Muthukumar, S.; Selvam, A. P.; Prasad, S. Flexible Nanoporous Tunable Electrical Double Layer Biosensors for Sweat Diagnostics. *Sci. Rep* **2015**, *5*, 1−11.
(50) Colucci, R.; Barbosa, H. F. D. P.; Günther, F.; Cavassin, P.; Faria, G. C. Recent Advances in Modeling Organic Electrochemical Transistors. *Flexible and Printed Electronics* **2020**, *5* (1), 013001.
(51) Bernards, D. A.; Macaya, D. J.; Nikolou, M.; Defranco, J. A.; Takamatsu, S.; Malliaras, G. G. Enzymatic Sensing with Organic Electrochemical Transistors. *J. Mater. Chem.* **2008**, *18*, 116−120.
(52) Bernards, B. D. A.; Malliaras, G. G. Steady-State and Transient Behavior of Organic Electrochemical Transistors. *Adv. Funct. Mater.* **2007**, *17*, 3538−3544.
(53) Romele, P.; Ghittorelli, M.; Kovács-Vajna, Z. M.; Torricelli, F. Ion Buffering and Interface Charge Enable High Performance Electronics with Organic Electrochemical Transistors. *Nat. Commun.* **2019**, *10* (1), 1−11.
(54) Bernards, D. A.; Malliaras, G. G. Steady-State and Transient Behavior of Organic Electrochemical Transistors. *Adv. Funct Mater.* **2007**, *17* (17), 3538−3544.
(55) Wu, H.; Ohnuki, H.; Murata, M.; Endo, H. Flow Immunosensor System with an Electrode Replacement Unit for Continuous Cortisol Monitoring for Fish. *Sens Biosensing Res.* **2017**, *13*, 122−127.
(56) Baker, L. B.; Wolfe, A. S. Physiological Mechanisms Determining Eccrine Sweat Composition. *Eur. J. Appl. Physiol* **2020**, *120*, 719−752.
(57) Rotman-Pikielny, P.; Rouach, V.; Chen, O.; Gur, H. G.; Limor, R.; Stern, N. Serum Cortisol Levels in Patients Admitted to the Department of Medicine: Prognostic Correlations and Effects of Age, Infection, and Comorbidity. *the American Journal of the Medical Sciences* **2006**, *332* (2), 61−67.

https://doi.org/10.1021/acssensors.2c01250
ACS Sens. 2022, 7, 2721−2731